

A DEEP SEARCH FOR PROMPT RADIO EMISSION FROM THE SHORT GRB 150424A WITH THE MURCHISON WIDEFIELD ARRAY

D. L. KAPLAN¹, A. ROWLINSON^{2,3,4,5}, K. W. BANNISTER^{2,3}, M. E. BELL^{2,3}, S. D. CROFT^{6,7}, T. MURPHY^{8,3}, S. J. TINGAY^{9,3},
R. B. WAYTH^{9,3}, A. WILLIAMS⁹,

ApJ Letters, in press

ABSTRACT

We present a search for prompt radio emission associated with the short-duration gamma-ray burst (GRB) 150424A using the Murchison Widefield Array (MWA) at frequencies from 80–133 MHz. Our observations span delays of 23 s–30 min after the GRB, corresponding to dispersion measures of 100–7700 pc cm^{−3}. We see no excess flux in images with timescales of 4 s, 2 min, or 30 min, and set a 3σ flux density limit of 3.0 Jy at 132 MHz on the shortest timescales: some of the most stringent limits to date on prompt radio emission from any type of GRB. We use these limits to constrain a number of proposed models for coherent emission from short-duration GRBs, although we show that our limits are not particularly constraining for fast radio bursts because of reduced sensitivity for this pointing. Finally, we discuss the prospects for using the MWA to search for prompt radio emission from gravitational wave transients and find that while the flux density and luminosity limits are likely to be very constraining, the latency of the gravitational wave alert may limit the robustness of any conclusions.

Subject headings: gamma-ray burst: general — gamma-ray burst: individual (150424A) — gravitational waves — radio continuum: general

1. INTRODUCTION

The Advanced LIGO interferometers (aLIGO; The LIGO Scientific Collaboration et al. 2015) have very recently started observational science runs, soon to be joined by other upgraded detectors. For the first time there is a realistic prospect for detection of an astrophysical gravitational wave (GW) transient, with a range of possible electromagnetic counterparts (Metzger & Berger 2012). Rapid multi-wavelength followup might then allow detection and characterization of astrophysical gravitational wave sources (see e.g., Singer et al. 2014; Kasliwal & Nissanke 2014), greatly enhancing the scientific utility of such a discovery. For instance, we might be able to conclusively determine the origin of short-duration GRBs (SGRBs; see Berger 2014 and Fong et al. 2015 for recent reviews) which are generally accepted to originate from neutron star-neutron star mergers.

Even before aLIGO begins operation, prompt radio followup of SGRBs may give clues as to their origin and help tie them to other mysterious phenomena. Specifi-

cally, a number of authors have suggested the possibility of prompt, coherent radio emission right before, during or right after neutron star-neutron star mergers through a variety of physical mechanisms (e.g., Usov & Katz 2000; Pshirkov & Postnov 2010). This may serve as an explanation (Totani 2013; Zhang 2014; Falcke & Rezzolla 2014) for Fast Radio Bursts (FRBs; Lorimer et al. 2007; Thornton et al. 2013): impulsive ms bursts of dispersed radio emission with peak flux densities of ∼ 1 Jy or more at 1.4 GHz and apparently cosmological origins.

Searches for prompt radio emission from GRBs have been conducted for decades but most have concentrated on the more-common long-duration GRBs (LGRBs) and/or not been very sensitive (see Obenberger et al. 2014 and Palaniswamy et al. 2014 for recent discussions). Observations that covered the times of the GRBs were usually from less-sensitive all-sky instruments (e.g., Dessenne et al. 1996; Obenberger et al. 2014), while more sensitive pointed observations often took several minutes to slew before starting to observe (e.g., Bannister et al. 2012; Palaniswamy et al. 2014). We instead take advantage of the capabilities of the Murchison Widefield Array (MWA; Lonsdale et al. 2009; Tingay et al. 2013) — a low frequency (80–300 MHz) interferometer located in Western Australia — for rapid, sensitive followup. With fully-electronic steering and a wide field-of-view, it can respond to astrophysical transients within 20 s of receiving an alert as we demonstrate below.

Here we present a search for prompt low-frequency radio emission associated with the short-duration GRB 150424A using the MWA. GRB 150424A was detected on 2015 April 25 at 07:42:57 UT by the Burst Alert Telescope (BAT) on board the *Swift* satellite (Gehrels et al. 2004; Beardmore et al. 2015). The γ-ray emission consists of multiple very bright pulses with a duration of about 0.5 s, followed by weak γ-ray emission up to 100 s after the initial pulses (Barthelmy et al. 2015).

¹ Department of Physics, University of Wisconsin–Milwaukee, Milwaukee, WI 53201, USA; kaplan@uwm.edu

² CSIRO Astronomy and Space Science (CASS), PO Box 76, Epping, NSW 1710, Australia

³ ARC Centre of Excellence for All-sky Astrophysics (CAASTRO)

⁴ Anton Pannekoek Institute for Astronomy, University of Amsterdam, Science Park 904, 1098 XH Amsterdam, The Netherlands

⁵ ASTRON, The Netherlands Institute for Radio Astronomy, Postbus 2, 7990 AA, Dwingeloo, The Netherlands

⁶ Astronomy Department, University of California, Berkeley, 501 Campbell Hall #3411, Berkeley, CA 94720, USA

⁷ Eureka Scientific, Inc., 2452 Delmer Street Suite 100, Oakland, CA 94602, USA

⁸ Sydney Institute for Astronomy, School of Physics, The University of Sydney, NSW 2006, Australia

⁹ International Centre for Radio Astronomy Research, Curtin University, Bentley, WA 6102, Australia

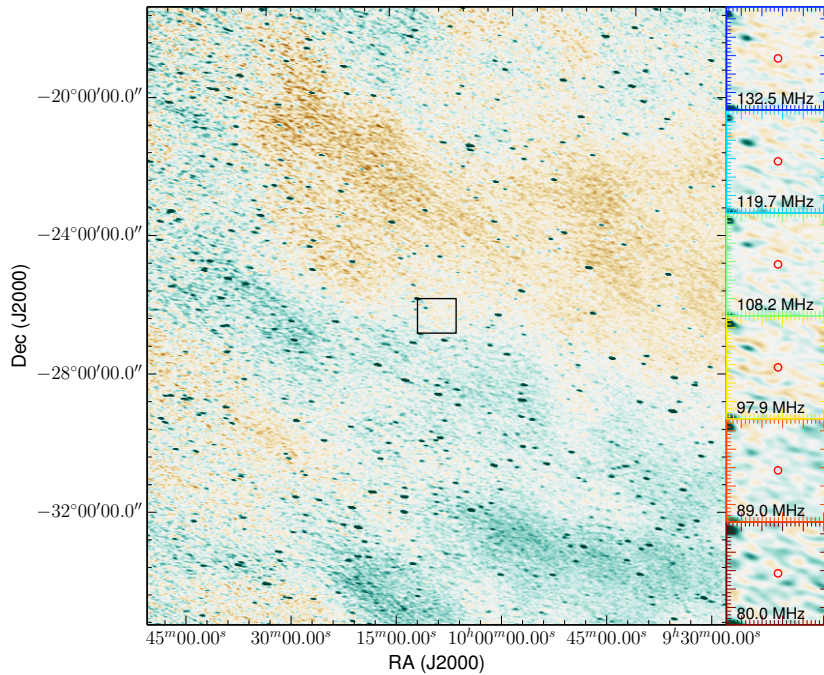


FIG. 1.— MWA image of the field of GRB 150424A. We show a $15^\circ \times 15^\circ$ portion of the 30 min mosaic in the 132.5 MHz sub-band. The box shows the sizes of the $1^\circ \times 1^\circ$ insets on the right, each of which shows the same portion of the field but for each sub-band (as labeled). The position of the GRB is indicated by the circle, and is known to $\ll 1$ pixel.

GRB 150424A is thus classified as a SGRB with extended emission (EE SGRB): a small population of GRBs whose properties are most consistent with SGRBs despite their long durations (e.g., Norris et al. 2010, 2011), and where the origin of the extended emission is still being debated but may involve a magnetar central engine (e.g., Metzger et al. 2008; Gompertz et al. 2014). The X-ray Telescope (XRT) began observing the location of GRB 150424A 87.9 s after the burst and found a bright, fading X-ray source. Followup observations (Castro-Tirado et al. 2015) identified a redshift $z = 0.3$ galaxy $5''$ (projected separation of 22.5 kpc) away from the optical afterglow (Perley & McConnell 2015). However, Tanvir et al. (2015) found a fainter potential host galaxy with a likely redshift of $z > 0.7$ underlying the GRB location. We note that the density of the medium surrounding this GRB is unknown and, if high, may impede the detection of coherent radio emission (Macquart 2007).

All cosmological quantities in this paper are computed based on Planck Collaboration et al. (2014). We use a nominal redshift of 0.7 for our calculations, consistent with Tanvir et al. (2015).

2. OBSERVATIONS & ANALYSIS

The MWA Monitor and Control computer received a socket-based notice from the Gamma-ray Coordinate Network (GCN) at 07:43:10 UT and quickly scheduled 30 min of observations of GRB 150424A. To save time, the telescope stayed in the same configuration as the previous observation which had been solar observing. This used an unusual configuration with the 24 coarse 1.28 MHz channels spread out in a “picket fence,” mode,

with 2.56 MHz sub-bands spread between 80 MHz and 240 MHz (and using 0.5 s correlator integrations with 40 kHz frequency resolution). Observations started at 07:43:20 UT, 23 s after the GRB. This was during the day at the MWA (Sun at 25° elevation) and with the GRB somewhat low in the sky (elevation 30°), although it was 123° away from the Sun. Because of the low elevation the MWA had less sensitivity and a more irregular primary beam shape than usual. The observations consisted of 15 individual 112 s scans, separated by 8 s.

The processing followed standard MWA procedures (e.g., Hurley-Walker et al. 2014). We performed initial phase calibration using an observation of Hydra A taken earlier in the same day in the same mode. We then imaged the scans with 4096×4096 $0.6''$ pixels in the XX and YY instrumental polarizations using **WSClean** (Offringa et al. 2014), using 40,000 CLEAN iterations and allowing for one round of amplitude and phase self-calibration (as demonstrated by Rowlinson et al. 2015, this does not remove transients as long as they do not dominate the total flux density of the image). Finally, we corrected the instrumental polarization to Stokes I (total intensity) using the primary beam from Sutinjo et al. (2015). The synthesized beam was elongated with an axis-ratio of 2.6:1 because of the low elevation; the major axis varied from $12'$ to $4.2'$ over the different sub-bands. Examining the images from the different sub-bands, the upper 6 sub-bands (frequencies ≥ 144 MHz) suffered significant image artifacts, mostly due to uncleaned sidelobes from Hydra A (18° to the north west of GRB 150424A) and primary beam grating lobes that encompassed the Sun. We ended up discarding the upper 6 sub-bands as we could not satisfactorily improve the image quality. For the remaining

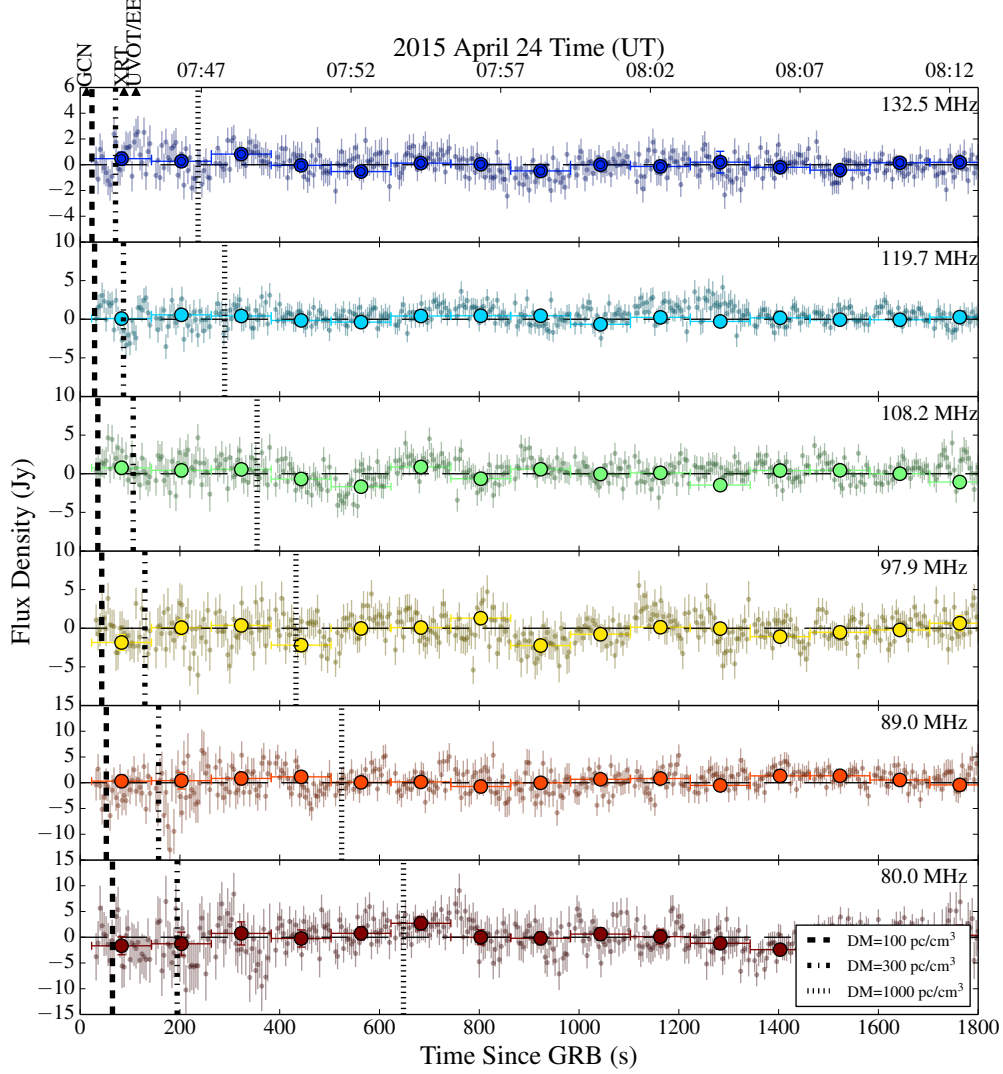


FIG. 2.— Flux densities at the position of GRB 150424A in each sub-band. We show measurements from the individual 4 s images (points) as well as 2 min images (circles). The black triangles in the top left corner show the times of the GCN, XRT, and UVOT observations as labeled; the time of the UVOT observation was also roughly the end of the extended emission (EE) period. We also show the appropriate delays relative to the time of the GRB for DMs of 100 pc cm^{-3} (dashed vertical lines), 300 pc cm^{-3} (dot-dashed vertical lines) and 1000 pc cm^{-3} (dotted vertical lines).

sub-bands, we combined individual 2 min scans into a single 30 min mosaic (as in Hurley-Walker et al. 2014); we show the mosaics for each sub-band in Figure 1. The flux density scale was corrected so that the bright, unresolved source PKS J0949–2511 ($4^{\circ}5'$ away from GRB) averaged over each 2 min observation matched the spectral energy distribution we interpolated from values from the NASA Extragalactic Database, given in Table 1. We then also created images with 4 s integration times, using the corrected uv data but only performing 100 CLEAN iterations on each.

For each set of images: 4 s, 2 min, and 30 min mosaics, we measured the flux density of PKS J0949–2511 along with the flux density at the position of the GRB (position uncertainty $\ll 1$ pixel; we verified that the position variation of PKS J0949–2511 due primarily to ionospheric refraction was $\lesssim 1$ pixel) and the image noise proper-

ties. In Figure 2 we show the flux densities at the position of GRB 150424A for each sub-band from both the 4 s and 2 min images. There is some degree of correlation between individual points (Bell et al. 2014), but as a whole the data are noise-like with reduced χ^2 values near 1 (0.76–0.98 depending on the band). We searched for statistically significant peaks in each of the sub-bands over a range of timescales from 4 s–2 min and see nothing exceeding 3σ , much less anything that is correlated between the sub-bands (with a possible delay allowing for interstellar dispersion). We then determined 3σ flux density limits, shown in Figure 3 and Table 1. Note that the 88.9 and 119.7 MHz sub-bands are slightly anomalous in that the limits from the 30 min mosaics are slightly worse than those from 2 min images. This may be from a combination of source confusion limiting the sensitivity of the mosaics and residual poorly-cleaned sidelobes

TABLE 1
REFERENCE FLUX DENSITIES AND 3- σ LIMITS

	80.0 MHz	88.9 MHz	97.9 MHz	108.1 MHz	119.7 MHz	132.5 MHz
Flux Density of PKS J0949–2511 (Jy).....	22.5	21.8	21.1	20.1	19.1	17.9
4 s Flux Density Limits for GRB 150424A (Jy)....	8.7	7.7	5.7	4.9	4.2	3.0
2 min Flux Density Limits for GRB 150424A (Jy) .	3.5	1.9	3.0	2.4	1.0	1.1
30 min Flux Density Limits for GRB 150424A (Jy)	2.6	2.4	1.9	1.4	1.3	0.9

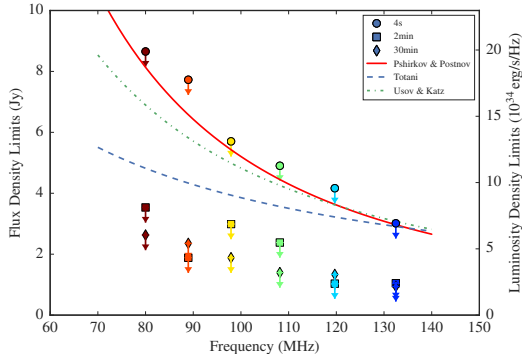


FIG. 3.— Flux density limits (3σ) for GRB 150424A in each sub-band, based on the 4 s images (circles), 2 min images (squares), and 30 min mosaics (diamonds); also see Table 1. We also show the luminosity density limits appropriate for a redshift $z = 0.7$; if the redshift is instead 0.3 (1), then the luminosities limits would decrease (increase) by a factor of 7 (2.4). We also show example predictions that have been adjusted to not exceed our 4 s limits from Pshirkov & Postnov (2010, with $\dot{E} \lesssim 5 \times 10^{50} \text{ erg s}^{-1}$ and assuming an efficiency scaling exponent $\gamma = 0$), Totani (2013, with efficiency $\epsilon_r \lesssim 5 \times 10^{-2}$, magnetic field $B = 10^{13} \text{ G}$ and initial spin period $P = 0.5 \text{ ms}$), and Usov & Katz (2000, with efficiency $\delta \lesssim 3.5 \times 10^{-7}$) appropriate for $\text{DM} < 444 \text{ pc cm}^{-3}$.

from Hydra A. As a whole, though, the 4 s sub-bands behave well, and the limits from the longer integrations are lower, almost by the factor of 5 expected from the integration time.

3. DISCUSSION

In our discussion of GRB 150424A, we consider how our observations constrain the potentially related phenomena of SGRBs and FRBs, and furthermore the implications of these results on low-frequency radio follow-up of GW transients. But first, we need to address the effects on any radio signal of propagation through intervening ionized media.

3.1. Propagation Effects

Any prompt radio signal from GRB 150424A is expected to be modified by its propagation through the interstellar medium (ISM) of its host galaxy, the intergalactic medium (IGM), and the ISM of the Milky Way (Macquart 2007). Free electrons will introduce dispersion, causing lower frequencies to arrive later while inhomogeneities will cause scattering that smears out temporal structure. Dispersion is quantified by the dispersion measure (DM): the integral of the line-of-sight electron density. We can expect a DM of about 80 pc cm^{-3} from the Milky Way (Cordes & Lazio 2002), and perhaps a roughly similar contribution from the GRB’s host galaxy. We expect the DM from the IGM to be roughly $1000 z \text{ pc cm}^{-3}$ for a redshift z (Inoue 2004; Trott et al. 2013), so we can expect $\text{DM}_{\text{IGM}} = 300 \text{ pc cm}^{-3}$ –

1000 pc cm^{-3} depending on the actual redshift of the GRB, and a total DM of 500 pc cm^{-3} – 1200 pc cm^{-3} . In Figure 2 we plot the time delays in each sub-band for a range of DMs. Even for the lowest possible DMs (just the Milky Way) our observing covered the delayed time of any prompt signal, especially in the lower sub-bands. Our 30 min observation spans the nominal DM range quite well, and we sample up to a DM of 2800 pc cm^{-3} for the lowest sub-band or 7700 pc cm^{-3} for the highest. Note that the dispersion across a bandpass of 2.56 MHz would last 9 s–40 s depending on the sub-band for a nominal DM of 1000 pc cm^{-3} , so a fast pulse would last 2–10 of our 4 s images. We assume that scattering does not significantly smear out any signal (Thornton et al. 2013; Lorimer et al. 2013; Macquart & Koay 2013), but note that this may need to be revisited as more information is gained about FRB behavior.

3.2. Short-Duration Gamma-Ray Bursts

Given the observed SGRB, we can constrain any associated prompt, coherent radio signal such as those predicted in models of neutron star-neutron star mergers (e.g., Pshirkov & Postnov 2010; Totani 2013) or more generic GRB phenomenon (e.g., Usov & Katz 2000). These models have poorly-predicted efficiency factors which we are able to constrain directly from our observations. We show example predictions that have been adjusted to not exceed our 4 s limits in Figure 3. For the rapid magnetized spin-down model of Pshirkov & Postnov (2010), we have spin-down luminosity $\dot{E} \lesssim 5 \times 10^{50} \text{ erg s}^{-1}$ and assume an efficiency scaling exponent $\gamma = 0$, while for the similar but lower B model of Totani (2013), we have efficiency $\epsilon_r \lesssim 5 \times 10^{-2}$, along with nominal magnetic field $B = 10^{13} \text{ G}$ and initial spin period $P = 0.5 \text{ ms}$. And for coherent radio emission from the magnetized wind of a magnetar central engine colliding with the ambient medium as in Usov & Katz (2000), we have ratio of radio to γ -ray fluence $\delta \lesssim 3.5 \times 10^{-7}$. Note that our constraints here are for a fixed observed timescale of 4 s, which limits the DM to 444 pc cm^{-3} for 133 MHz observations. At higher DMs, our constraints will scale up accordingly. These constraints will be explored further in Rowlinson et al. (2015b in prep). With a detection we can use the fluence, duration, and delay of any coherent emission to strongly constrain any model.

In Figure 4 we compare our observations to other GRB searches from the literature. To compare observations at a range of frequencies and timescales, we convert them to a common sensitivity assuming $S_\nu \propto \nu^{-2}$ (e.g., Pshirkov & Postnov 2010) and that sensitivity scales as $1/\sqrt{\delta t}$ (with δt the integration time). We see that our limits are a factor of ~ 10 – 100 deeper than those from Bannister et al. (2012, assuming no detections) or Obenberger et al. (2014), and cover far closer to the time of the GRB than

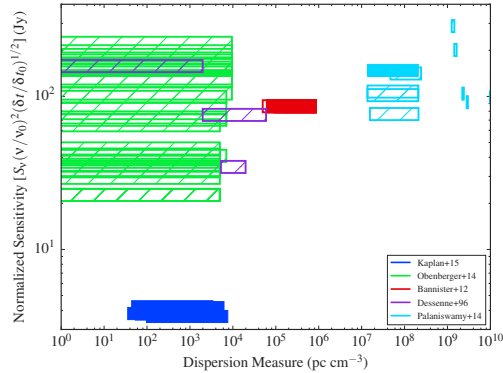


FIG. 4.— Limits to prompt emission from GRBs, based on Obenberger et al. (2014, 38–74 MHz; green), Bannister et al. (2012, 1400 MHz; red), Dessenne et al. (1996, 151 MHz; purple), Palaniswamy et al. (2014, 2300 MHz; cyan), and this paper (blue). The follow-up times have been converted into an effective dispersion measure, assuming that the radio emission is coincident with the GRB. The flux density limits have been normalized by frequency (assuming $S_\nu \propto \nu^{-2}$; e.g., Pshirkov & Postnov 2010) to $\nu_0 = 100$ MHz and to a common timescale of $\delta t_0 = 10$ s. Short-duration GRBs — those listed as such in the literature — are filled shapes, while long-duration GRBs are hatched. The same GRB can be shown multiple times if it was observed at different telescopes/frequencies. For comparison, FRBs are detected at DMs of $400\text{--}1100\text{ pc cm}^{-3}$ with 1.4-GHz peak flux densities of ~ 1 Jy over a ~ 10 ms pulse (Keane & Petroff 2015): scaled to a 10-s observation this would be a factor of $\sim 10^3$ too low to display here.

the former.

3.3. Fast Radio Bursts

Some of the models for FRBs tie them directly to neutron star-neutron star mergers and SGRBs (e.g., Totani 2013; Zhang 2014). For example, Zhang (2014) predict a FRB when a magnetar central engine powering the GRB collapses to form a black hole, which might happen at the end of the extended emission phase (Lü et al. 2015, but see Gompertz et al. 2014). Since our observations cover from right after the GRB (allowing for dispersion) to well past the end of the extended emission, we can place the first constraints on this model for the extended emission.

In our most sensitive sub-bands of 133 MHz, we set a 3σ limit to the flux density of any short-duration emission of < 3.0 Jy. This translates into a fluence limit of < 12.0 Jys, compared to FRB fluences at 1.4 GHz of < 1 Jy ms to > 30 Jy ms (Keane & Petroff 2015). Assuming flux densities scale $S_\nu \propto \nu^\alpha$, we can only exclude FRBs with spectral indices $\alpha < -2.5$. This is not particularly constraining (unlike Karastergiou et al. 2015; Tingay et al. 2015; Rowlinson et al. 2015), largely because of the reduced sensitivity of the MWA at this low elevation (cf. Trott et al. 2013) and with the contribution of the Sun to the system temperature. It is also possible that the 1.4-GHz FRB detections have been aided by interstellar scintillation (Macquart & Johnston 2015) which would not help at these frequencies.

3.4. Gravitational Wave Transients

Finally, we can consider the constraints on GW transients. The aLIGO detectors were not operating during GRB 150424A, so no direct GW limit can be determined, but we can consider the prospects for MWA followup of

GW transients. As discussed in Singer et al. (2014), the error regions for GW triggers in 2015–2016 can cover hundreds of square degrees. Moreover, they need not be compact or simply connected. While the nominal field-of-view of the MWA is about 600 deg^2 at 150 MHz, we cannot always cover all of the expected error regions. Unless the GW event occurs within the MWA’s field-of-view (chance of $\approx 1\%$), we will need to re-point following a GW trigger.

Given the expected range of redshift/DM for GW events (intergalactic DMs of $10\text{--}50\text{ pc cm}^{-3}$, or total DMs of $50\text{--}200\text{ pc cm}^{-3}$), we expect time delays from the GW event of only $41(\nu/100\text{ MHz})^{-2}(\text{DM}/100\text{ pc cm}^{-3})$ s, not including possible internal delays (Zhang 2014). As we have demonstrated, 20 s is sufficient for MWA followup, but the bigger question is the latency of the GW detection and notice. Currently the low-latency compact binary coalescence pipeline is expected to send out notices with a time delay of 90–120 s after the GW event (Singer et al. 2014; Cadonati et al. 2014), although this could decrease as the signal-to-noise increases, with a detection potentially even occurring before the merger (Cannon et al. 2012). Although this can be mitigated at some level by moving to frequencies $\lesssim 60$ MHz where the dispersive delay increases to surpass the GW event delay this delay may ultimately be a significant limitation for the prospects of prompt GW followup (Chu et al. 2015).

If we are able to point appropriately, we expect a limiting flux density of about 0.1 Jy, or luminosity limits of $10^{38\text{--}39}\text{ erg s}^{-1}$ for typical distances. Since GW sources would be at redshifts < 0.05 compared to 0.3–1 here, any radio emission would be significantly brighter by a factor of 50–1000. This would lead to much more realistically constraining models for FRBs and SGRBs, with e.g., ϵ_r from Totani (2013) close to the value of 10^{-4} seen for radio pulsars, or an \dot{E} from Pshirkov & Postnov (2010) close to the range inferred from modeling extended emission in SGRBs (Gompertz et al. 2015).

4. CONCLUSIONS

We have demonstrated prompt followup with a pointed radio telescope that we have used to set stringent limits to any prompt, coherent emission from the short GRB 150424A. Looking on our fastest timescale of 4 s, we set 3σ flux density limits of 3.0 Jy at 133 MHz. These limits are a factor of ~ 100 lower than most prior limits, and cover delays of 23 s–30 min after the GRB, corresponding to DMs of $100\text{--}7700\text{ pc cm}^{-3}$. We did not detect any FRB coincident with the GRB, but these limits are not very constraining compared to the population of FRBs because of reduced sensitivity for this particular pointing.

We plan to continue our GRB followup program over the next year, although given the preferred elevation range of $> 45^\circ$ the rate of *Swift* SGRBs suitable for MWA followup is $< 1\text{ yr}^{-1}$. However, this serves as a demonstration and template analysis for future followup of GW transients — particularly timely given the very recent start of science runs with the aLIGO detectors. We will work to improve the analysis time for the MWA data to facilitate multi-wavelength followup over the large GW error regions (Singer et al. 2014). Additional work in reducing the latency of the GW triggers will also be helpful

since that is expected to be a limitation on the robustness of any conclusions from low-frequency radio searches.

We thank an anonymous referee for useful comments and J.-P. Macquart, C. Trott, A. Urban, A. Offringa, and S. B. Cenko for helpful discussions. This work uses the Murchison Radio-astronomy Observatory, operated by CSIRO. We acknowledge the Wajarri Yamatji people as the traditional owners of the Observatory site. Support for the operation of the MWA is provided by the Australian Government Department of Industry and Science and Department of Education (National Collaborative Research Infrastructure Strategy: NCRIS), under a con-

tract to Curtin University administered by Astronomy Australia Limited. We acknowledge the iVEC Petabyte Data Store and the Initiative in Innovative Computing and the CUDA Center for Excellence sponsored by NVIDIA at Harvard University. DLK and SDC are additionally supported by NSF grant AST-1412421. This research made use of APLpy, an open-source plotting package for Python hosted at <http://aplpy.github.com>. This research has made use of the NASA/IPAC Extragalactic Database (NED), which is operated by the Jet Propulsion Laboratory, California Institute of Technology, under contract with the National Aeronautics and Space Administration.

Facilities: Murchison Widefield Array.

REFERENCES

- Bannister, K. W., Murphy, T., Gaensler, B. M., & Reynolds, J. E. 2012, *ApJ*, 757, 38
- Barthelmy, S. D., Baumgartner, W. H., Beardmore, A. P., et al. 2015, GRB Coordinates Network, 17761, 1
- Beardmore, A. P., Page, K. L., Palmer, D. M., & Ukwatta, T. N. 2015, GRB Coordinates Network, 17743, 1
- Bell, M. E., Murphy, T., Kaplan, D. L., et al. 2014, *MNRAS*, 438, 352
- Berger, E. 2014, *ARA&A*, 52, 43
- Cadonati, L., Astone, P., & van den Broeck, C. 2014, The LSC-Virgo White Paper on Gravitational Wave Searches and Astrophysics, Tech. Rep. T1400054-v7, LIGO, <https://dcc.ligo.org/LIGO-T1400054/public>
- Cannon, K., Cariou, R., Chapman, A., et al. 2012, *ApJ*, 748, 136
- Castro-Tirado, A. J., Sanchez-Ramirez, R., Lombardi, G., & Rivero, M. A. 2015, GRB Coordinates Network, 17758, 1
- Chu, Q., Howell, E. J., Rowlinson, A., Gao, H., Zhang, B., Tingay, S. J., Boër, M., & Wen, L. 2015, *MNRAS*, submitted, arXiv:1509.06876
- Cordes, J. M. & Lazio, T. J. W. 2002, arXiv:astro-ph/0207156
- Dessenne, C. A.-C., Green, D. A., Warner, P. J., et al. 1996, *MNRAS*, 281, 977
- Falcke, H. & Rezzolla, L. 2014, *A&A*, 562, A137
- Fong, W.-F., Berger, E., Margutti, R., & Zauderer, B. A. 2015, *ApJ*, submitted, arXiv:1509.02922
- Gehrels, N., Chincarini, G., Giommi, P., et al. 2004, *ApJ*, 611, 1005
- Gompertz, B. P., O’Brien, P. T., & Wynn, G. A. 2014, *MNRAS*, 438, 240
- Gompertz, B. P., van der Horst, A. J., O’Brien, P. T., Wynn, G. A., & Wiersema, K. 2015, *MNRAS*, 448, 629
- Hurley-Walker, N., Morgan, J., Wayth, R. B., et al. 2014, *PASA*, 31, 45
- Inoue, S. 2004, *MNRAS*, 348, 999
- Karastergiou, A., Chennamangalam, J., Armour, W., et al. 2015, *MNRAS*, 452, 1254
- Kasliwal, M. M. & Nissanke, S. 2014, *ApJ*, 789, L5
- Keane, E. F. & Petroff, E. 2015, *MNRAS*, 447, 2852
- Lonsdale, C. J., Cappallo, R. J., Morales, M. F., et al. 2009, *IEEE Proceedings*, 97, 1497
- Lorimer, D. R., Bailes, M., McLaughlin, M. A., Narkevic, D. J., & Crawford, F. 2007, *Science*, 318, 777
- Lorimer, D. R., Karastergiou, A., McLaughlin, M. A., & Johnston, S. 2013, *MNRAS*, 436, L5
- Lü, H.-J., Zhang, B., Lei, W.-H., Li, Y., & Lasky, P. D. 2015, *ApJ*, 805, 89
- Macquart, J.-P. 2007, *ApJ*, 658, L1
- Macquart, J.-P. & Johnston, S. 2015, *MNRAS*, 451, 3278
- Macquart, J.-P. & Koay, J. Y. 2013, *ApJ*, 776, 125
- Metzger, B. D. & Berger, E. 2012, *ApJ*, 746, 48
- Metzger, B. D., Quataert, E., & Thompson, T. A. 2008, *MNRAS*, 385, 1455
- Norris, J. P., Gehrels, N., & Scargle, J. D. 2010, *ApJ*, 717, 411
- . 2011, *ApJ*, 735, 23
- Obenberger, K. S., Hartman, J. M., Taylor, G. B., Craig, J., Dowell, J., Helmboldt, J. F., Henning, P. A., Schinzel, F. K., & Wilson, T. L. 2014, *ApJ*, 785, 27
- Offringa, A. R., McKinley, B., Hurley-Walker, N., et al. 2014, *MNRAS*, 444, 606
- Palaniswamy, D., Wayth, R. B., Trott, C. M., McCallum, J. N., Tingay, S. J., & Reynolds, C. 2014, *ApJ*, 790, 63
- Perley, D. A. & McConnell, N. J. 2015, GRB Coordinates Network, 17745, 1
- Planck Collaboration et al. 2014, *A&A*, 571, A16
- Pshirkov, M. S. & Postnov, K. A. 2010, *Ap&SS*, 330, 13
- Rowlinson, A., Bell, M. E., Murphy, T., et al. 2015, *MNRAS*, submitted
- Singer, L. P., Price, L. R., Farr, B., et al. 2014, *ApJ*, 795, 105
- Sutinjo, A., O’Sullivan, J., Lenc, E., Wayth, R. B., Padhi, S., Hall, P., & Tingay, S. J. 2015, *Radio Science*, 50, 52
- Tanvir, N. R., Levan, A. J., Fruchter, A. S., et al. 2015, GRB Coordinates Network, 18100, 1
- The LIGO Scientific Collaboration et al. 2015, *Classical and Quantum Gravity*, 32, 074001
- Thornton, D., Stappers, B., Bailes, M., et al. 2013, *Science*, 341, 53
- Tingay, S. J., Goeke, R., Bowman, J. D., et al. 2013, *PASA*, 30, 7
- Tingay, S. J., Trott, C. M., Wayth, R. B., et al. 2015, *AJ*, in press, arXiv:1511.02985
- Totani, T. 2013, *PASJ*, 65, L12
- Trott, C. M., Tingay, S. J., & Wayth, R. B. 2013, *ApJ*, 776, L16
- Usov, V. V. & Katz, J. I. 2000, *A&A*, 364, 655
- Zhang, B. 2014, *ApJ*, 780, L21